Magnetic and structural properties of fcc/hcp bi-crystalline multilayer Co nanowire arrays prepared by controlled electroplating

K. R. Pirota, F. Béron, D. Zanchet, T. C. R. Rocha, D. Navas et al.

Citation: J. Appl. Phys. **109**, 083919 (2011); doi: 10.1063/1.3553865
View online: http://dx.doi.org/10.1063/1.3553865
View Table of Contents: http://jap.aip.org/resource/1/JAPIAU/v109/i8
Published by the AIP Publishing LLC.

Magnetic and structural properties of fcc/hcp bi-crystalline multilayer Co nanowire arrays prepared by controlled electroplating

K. R. Pirota,[1,a)] F. Béron,[1] D. Zanchet,[2] T. C. R. Rocha,[2] D. Navas,[3] J. Torrejón,[1] M. Vazquez,[3] and M. Knobel[1]
[1]*Instituto de Física Gleb Wataghin, Universidade Estadual de Campinas (UNICAMP), 13083-970, Campinas (SP), Brazil*
[2]*Laboratório Nacional de Luz Sincrotron (LNLS), 13083970, Campinas (SP), Brazil*
[3]*Instituto de Ciencia de Materiales de Madrid, CSIC, 28049 Madrid, Spain*

(Received 28 September 2010; accepted 8 January 2011; published online 21 April 2011)

We report on the structural and magnetic properties of crystalline bi-phase Co nanowires, electrodeposited into the pores of anodized alumina membranes, as a function of their length. Co nanowires present two different coexistent crystalline structures (fcc and hcp) that can be controlled by the time of pulsed electrodeposition. The fcc crystalline phase grows at the early stage and is present at the bottom of all the nanowires, strongly influencing their magnetic behavior. Both structural and magnetic characterizations indicate that the length of the fcc phase is constant at around 260–270 nm. X-ray diffraction measurements revealed a strong preferential orientation (texture) in the (1 0–1 0) direction for the hcp phase, which increases the nanowire length as well as crystalline grain size, degree of orientation, and volume fraction of oriented material. The first-order reversal curve (FORC) method was used to infer both qualitatively and quantitatively the complex magnetization reversal of the nanowires. Under the application of a magnetic field parallel to the wires, the magnetization reversal of each region is clearly distinguishable; the fcc phase creates a high coercive contribution without an interaction field, while the hcp phase presents a smaller coercivity and undergoes a strong antiparallel interaction field from neighboring wires. © *2011 American Institute of Physics*. [doi:10.1063/1.3553865]

I. INTRODUCTION

Progress in advanced electronics, magnetic sensors, and information storage devices relies on continued miniaturization of their components as well as on the development of novel materials and less-expensive alternative technologies. In particular, magnetic nanowires represent a kind of system where intrinsic shape together with crystalline anisotropy can be successfully exploited in a number of applications.[1–3] For example, in the case of nanowire arrays, each single-domain nanowire could represent one bit of information, depending on its magnetization state,[4,5] and thus these wires have high potential for magnetic storage of information. Alternatively, controlled propagation of domain walls in ordered arrays of submicrometer wires can be employed for information propagation in magnetoelectronic devices, such as those proposed for magnetic memory technology.[6,7] These perspectives have encouraged the fabrication of ordered magnetic nanoelement arrays displaying uniaxial magnetic anisotropy. In this regard, a deeper understanding of the reversal mechanism of such nanowires represents an important challenge for the optimization of such technologies.

An alternative approach for preparation of magnetic nanowires based on electroplating of magnetic metals and alloys into self-assembled pores of anodic alumina membranes (AAM) is being increasingly employed.[8] This method enables the less-expensive preparation of arrays of parallel nanowires showing a 2D-polycrystalline arrangement of hexagonal symmetry. The magnetic behavior of these arrays is determined by the magnetic anisotropy of individual nanowires—that is, shape plus magnetocrystalline contributions—together with the magnetostatic interactions among nanowires. In the case of Ni, Pt, and Fe nanowires with large length-to-diameter aspect ratios the shape anisotropy typically overcomes the magnetocrystalline contribution and determines an easy magnetization direction parallel to the wire axes.[9–12] For example, Ni nanowires present a crystal anisotropy constant of about 10^3 J/m^3, with an easy axis perpendicular to the wire axis (fcc phase), while the longitudinal shape anisotropy constant of an individual nanowire takes a value of $\pi\mu_0 M_s^2 = 7 \times 10^4$ J/m^3, which favors a resultant axial easy axis.

In turn, Co presents a much stronger magnetocrystalline anisotropy that completely modifies this picture. It is known that Co nanowires usually crystallize in the hexagonal close packing (hcp) phase, with the cubic (fcc) structure less common. The hexagonal symmetry axis (c) of the hcp phase, perpendicular to the wire axis, favors a transverse magnetization easy axis, and its crystalline anisotropy constant ($\sim 5 \times 10^5$ J/m^3 for bulk) nearly compensates for the shape anisotropy ($\pi\mu_0 M_s^2 = 6 \times 10^5$ J/m^3). This energetic balance leads, for example, to a significantly reduction of the longitudinal remanence. Also, it is worth noting that the out-of-equilibrium fcc phase exhibits an easy axis nearly parallel

a)Electronic mail: krperota@ifi.unicamp.br.

to the wire axis.[13] The structure of electrodeposited Co nanowires strongly depends on numerous parameters such as bath composition, electrolyte pH, deposition current density, deposition temperature, and agitation.[14] The geometry (i.e., their diameter) can also determine the crystalline structure of Co nanowires.[15] A novel method to grow fcc Co with easy axis nearly parallel to the wire axis in out-of-equilibrium state has been reported.[16] Therefore, short and long Co nanowires (i.e., short and long electroplating time) are expected to present fcc and a mixture of fcc and hcp phases, respectively.

In this work, we have prepared Co nanowires by electroplating and filling of self-assembled 35 nm diameter nanopores of anodized alumina membranes with lengths on the micrometer scale. The structure and magnetic properties were subsequently characterized. These nanowires present a heterogeneous crystalline structure, with a short fcc phase at the bottom, followed by a longer hcp phase. Their total length was chosen so that both contributions were nonnegligible. The results extracted from synchrotron X-ray diffraction are complemented with those from major hysteresis curves and first-order reversal curve (FORC) techniques.[17–19] This latter method allows one to examine the magnetic properties of individual nanowires as well as the nature of the interactions among them, making use of simple measurements in a vibration sample magnetometer (VSM). All characterization techniques confirmed the suspected fcc/hcp phase structure and the FORC characterization was able to separate the two different magnetic contributions from the hcp and fcc phases. This kind of material could also be applied as a new class of exchange spring system, one that combines hard and soft magnetic properties in a unique layered system.[20]

II. EXPERIMENTAL DETAILS

Anodic alumina membranes, AAM, were prepared in a two-step anodization process.[10] High-purity aluminum (Goodfellow, 99.999%) foils were degreased, cleaned, dried, and finally electropolished. The anodization procedure was performed using 0.3 M of oxalic acid solution as the electrolyte, applying a voltage of 40 V and keeping the temperature constant at 2 °C. The first anodization time, which determines the final hexagonal order degree, was fixed at 24 h. After anodization the porous oxide was removed using a phosphoric acid solution. The valleys of the remaining nanostructure pattern printed on the aluminum surface play the role of starting nucleation points for pore growth during the second anodization process, which lasted for 2 h, leading to a total pore length of about 4.5 μm. The final porous alumina presents a hexagonal array of pores with diameter of 35 nm and an interpore distance of about 105 nm.

The growth of Co nanowires inside the pores was carried out in a homemade electrochemical cell using a Watts bath at a constant temperature of 40 °C. The pulsed electrodeposition method consisted of a 2 ms current pulse of −30 mA followed by a 2 ms positive voltage pulse of 5 V. That pulse sequence was repeated after 1 s of null current and voltage. The total electrodeposition time was varied between 30 and 60 min, which resulted in nanowires with length L ranging from 1125 to 2250 nm. Morphological studies were first performed by high-resolution scanning electron microscopy (HRSEM).

Synchrotron X-ray diffraction (XRD) was used to investigate the crystallographic phase and texture of the Co nanowires. The experiments were performed at the Laboratorio Nacional de Luz Sincroton (LNLS), Campinas, Brazil, with an XRD2 beam line using reflection geometry with 1.6314 Å radiation, below the Co absorption edge to avoid Co fluorescence. For each array, a conventional θ–2θ curve was obtained together with rocking curves (detector angle fixed and sample scanned) for two peaks. For all curves given below, the 2θ values were rescaled for Cu K-α radiation (1.54056 Å). Peak width analysis was performed by fitting a pseudo-Voigt function, and the mean crystallite sizes were estimated by the Scherrer equation. The rocking curve data were corrected using TexturePlus software[21] to eliminate background and absorption effects and then fitted to the March-Dollase profile function[22] to quantify the texture distributions from the rocking curves. For multiple random distributions, the single parameter cylindrical texture function is given by $(r^2\cos^2\omega + r^{-1}\sin^2\omega)^{-3/2}$, where ω is the angle between the texture axis and the scattering vector, and r is the degree of orientation of oriented material, which ranges from 1 (randomly oriented grains) to 0 (perfectly textured grains). Randomly oriented grains produce a constant rocking curve, whereas textured grains produce a peaked curve. Finally, the volume fraction of oriented material was obtained by dividing the peak area by the total rocking curve area, after subtracting the background area coming from the random contributions.

The magnetization process was studied with VSM magnetometer under an applied magnetic field of 1.6×10^6 A/m maximum amplitude, both longitudinal and perpendicular to the wire axis. The analysis of distributed magnetic parameters of the hysteresis loops was performed through first-order reversal curves (FORCs). The FORC diagrams were obtained from a set of several minor hysteresis loops after magnetic saturation under a large positive field. The field is then ramped down to a given reversal field H_r. The FORC is the measured magnetization M as the field H is increased from H_r back to the saturation. The FORC distribution is obtained from a mixed second derivative of the magnetization[17]:

$$\rho(H, H_r) = -\frac{1}{2}\frac{\partial^2 M(H, H_r)}{\partial H \partial H_r} \qquad (H \geq H_r). \tag{1}$$

An extrapolated FORC diagram is the contour plot of a FORC distribution, where the experimental curves have been previously extrapolated in the $H < H_r$ region in a way to minimize discontinuities at $H = H_r$. The abscissa and ordinate coordinates are conveniently substituted by $[H_c = (H_r - H)/2, H_u = -(H_r + H)/2]$. According to the classical Preisach model, the FORC distribution represents the statistical distribution of square hysteresis curves (coercivity $= H_c$, bias field $= H_u$) called mathematical hysterons.[17] However, it is also possible to apply the FORC method to systems that do not satisfy the conditions of this

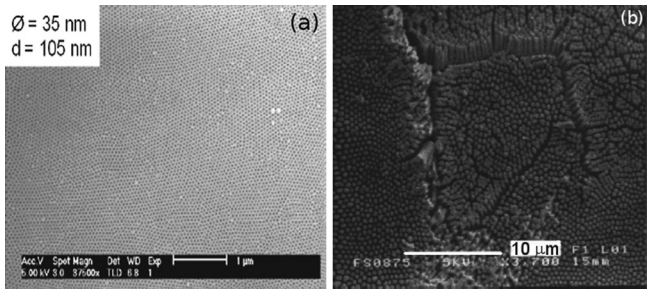

FIG. 1. HRSEM images of the sample surface top view: (a) as fabricated, and (b) after partial dilution of the alumina matrix.

simple model, which is the case for most magnetic systems. The analysis of results therefore can be achieved using a physical analysis model.[19] By its nature, the FORC method allows one to deconvolute individual from global properties, i.e., obtain both the coercivity and the interaction field of magnetic entities in a system. These features make it a really advantageous characterization technique for nanowire arrays, because of their large interaction field. It was successfully used to quantify the interaction field at saturation and the individual nanowire coercivity of Ni and CoFeB nanowire arrays.[23,24]

III. RESULTS AND DISCUSSION

A. Morphological and structural characterization

Figure 1(a) shows the AAM surface where the hexagonal order degree and the homogeneity of the pores can be observed. Figure 1(a) reveals the presence of uniform pores with a diameter of 35 nm, arranged with hexagonal symmetry and a lattice constant (or interpore distance) of about 105 nm. A partial dilution of the alumina matrix with 1 M NaOH solution allows one to observe the high quality of the deposited Ni nanowires [Fig. 1(b)].

All samples exhibit similar synchrotron X-ray diffraction curves to the one shown in Fig. 2(a) for Co nanowire array with $L = 1700$ nm. The positions of the strongest peak positions are consistent with an hcp lattice, which is the equilibrium phase of bulk Co. The additional peak located around 44.5° can be indexed either as the (0002) direction of the hcp phase or as the (1 1 1) direction of the fcc phase. We ascribe it to the fcc structure since previous XRD experiments on Co nanowires showed that this peak does not appear for the almost homogeneous hcp phase, while it is clearly visible for pure fcc phase nanowires.[16] Finally, the most intense peak is assigned to the Al substrate. The peaks are indexed according to this identification. The respective hcp mean crystallite size d for each array was derived from the peak widths (see Table I). From a quantitative analysis of results we deduce that nanowires show polycrystalline structure in all arrays, and that the crystallite size increases with nanowire length.

On the other hand, the relative peak intensity does not agree with expected intensities for an hcp lattice. The experimental intensity ratio of Co(1 0–1 0)/Co(1 0–1 1) peaks is larger than the expected value by a factor of 10, which indicates the presence of a strong preferential orientation (texture) in the Co(1 0–1 0) direction. In order to better address this texture, rocking curves were obtained for the (10–10) and (1 0–1 1) peaks [inset of Fig. 2(a), $L = 1700$ nm]. The rocking curve for a statistically perfect powder (uniformly random oriented crystallites) should be flat, since for any position of the sample there should be the same number of crystallites fulfilling the Bragg condition. The (1 0–1 1) rocking curve presents only a broad peak at low angles due to variations in the irradiated volume and absorption of the sample. However, the curve for the (1 0–1 0) peak presents a well-defined peak close to the specular value, confirming the strong preferential orientation. Thus, the hexagonal unit cell plane lies normal to the sample plane and consequently, the c direction is perpendicular to the nanowire axes.

Figure 2(b) presents the normalized rocking curves using the (1 0–1 0) reflection for the 1125, 1700, and 2250 nm long Co nanowire arrays. As observed, all curves exhibit a well-defined peak with different widths, reflecting variations in the degree of orientation (r), and slightly different positions related to the angle between the preferred orientation axis and the sample normal (ω_0). Moreover, the curves tend to different constant values at higher angles which indicates that the fraction of oriented material (f) differs for different samples, since randomly oriented grains give rise to a constant rocking curve. The texture quantification for each sample was performed by fitting the rocking curve using the March-Dollase function (Table I). The inset in Fig. 2(b) shows the fitted curve for $L = 1125$ nm, obtained from the rocking curve, after correction for the absorption and irradiated volume. As observed, a fairly good fit was obtained.

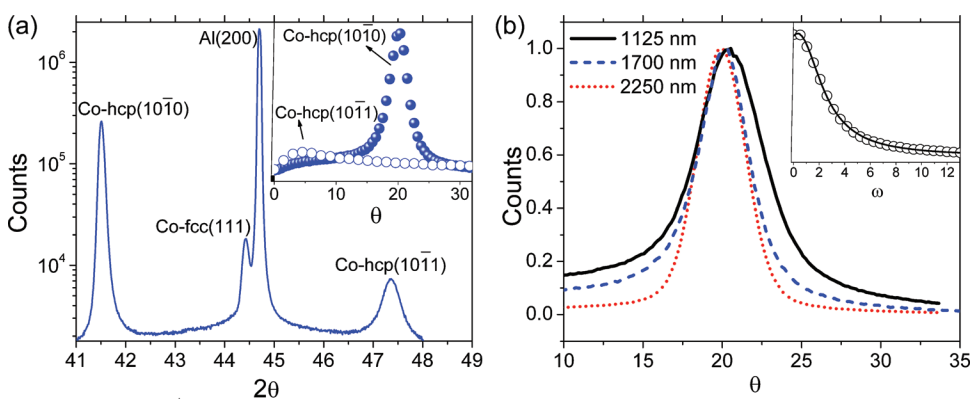

FIG. 2. (Color online) X-ray characterization of the Co nanowire arrays. (a) Complete X-ray pattern, inset: rocking curves for the 1 0 – 1 0 (black dots) and 1 0 – 1 1 (open dots) peaks ($L = 1700$ nm). (b) 1 0–1 0 rocking curves. Inset: Fit with the ω curve ($L = 1125$ nm).

TABLE I. Total nanowire length (L), hcp mean crystallite size (d), degree of orientation (r), volume fraction of oriented material (f), angle between the texture axis and sample normal (ω_0), and fcc phase length calculated from structural results (L_{fcc}), with estimated errors.

L (nm)	d (nm)	r	f (%)	ω_0 (degrees)	L_{fcc} (nm)
2250	29 ± 5	0.11 ± 0.01	98 ± 1	0.57 ± 0.01	50 ± 20
1700	27 ± 5	0.12 ± 0.02	83 ± 2	0.22 ± 0.01	290 ± 30
1125	25 ± 6	0.15 ± 0.02	79 ± 2	0.87 ± 0.01	240 ± 20

A quantitative analysis of the structural data of the hcp phase shows a clear correlation between the length of the nanowires and the volume fraction of oriented material, degree of orientation, and crystallite size. The values for the texture axis angle ω_o, all lying below 1°, confirm that the hcp c axis is perpendicular to the nanowire axis. This correlation agrees with the assumption that the Co nanowires present a mixture of fcc and hcp phases, both found in the XRD pattern. The fcc phase, only formed during the early stage of electrodeposition, should present a constant length for arrays deposited with identical parameters. Therefore, as the nanowire length increases, the fraction of the fcc contribution decreases, leading to a more oriented polycrystalline hcp signal. The structural fcc phase length (L_{fcc}) was calculated from the volume fraction of oriented material, assuming that only hcp and fcc phases are present (Table I). L_{fcc} values are similar for all samples with different length, giving a mean value of around 260 nm, except the result extracted from $L = 2250$ nm, which was a smaller value. This discrepancy could arise from the accuracy of the fit of the rocking curve when the fraction of the predominant texture is almost 100%.

B. Magnetic characterization

Figure 3 shows hysteresis loops for the studied Co nanowire arrays. As observed, the three arrays present an overall longitudinal easy axis indicating that the axial anisotropy from the nanowire shape and the fcc phase overcomes the perpendicular anisotropy of the hcp phase. It is important to note that for the latter, while the longitudinal direction is a hard crystalline magnetic axis, the perpendicular one does not represent an easy axis because of its polycrystalline structure.

Despite the fact that major hysteresis curves reflect the magnetic behavior of the whole nanowire array, they can be used to extract interesting information about heterogeneous two-phase nanowires. Neglecting the interaction field among nanowires, the remanent magnetization of the fcc phase is expected to remain aligned after longitudinal magnetic saturation, being along an easy axis, while the hcp phase remanence should be independent of the nanowire length. This behavior can be used to evaluate the length of the fcc phase nanowire pieces by plotting the normalized remanence as a function of the inverse nanowire length (Fig. 4). A surface or extremity effect will lead to a linear dependence if the thickness of the fixed magnetization portion remains constant. The remanence can be expressed as the addition of contributions from each phase as:

$$V\frac{M_r}{M_s} = V_{fcc}\frac{M_{r-fcc}}{M_s} + V_{hcp}\frac{M_{r-hcp}}{M_s}, \tag{2}$$

where V_i and M_{r-i} represent, respectively, the volume and the fractional remanent magnetization of each crystalline phase. Since the nanowire cross section is constant, taking the remanent magnetization percentage of the fcc phase as 100% Eq. (2) be rearranged as:

$$\frac{M_r}{M_s} = \frac{L_{fcc}}{L} \times 1 + \frac{L_{hcp}}{L}\frac{M_{r-hcp}}{M_s}. \tag{3}$$

Finally, considering that $L = L_{fcc} + L_{hcp}$, Eq. (3) becomes:

$$\frac{M_r}{M_s} = L_{fcc}\frac{1}{L}\left(1 - \frac{M_{r-hcp}}{M_s}\right) + \frac{M_{r-hcp}}{M_s}. \tag{4}$$

From the linear fit of Fig. 4, the magnetic fcc phase length is estimated to be $L_{fcc} = 273 \pm 7$ nm, which is near the mean value calculated from the structural characterization. It corresponds to about 7 min of electrodeposition time, according to previous calibrations. For the hysteresis loops under a perpendicular applied field, no such behavior of fixed magnetization was found.

Further magnetic characterization has been achieved with the help of FORC technique. Its sensitivity allows for the extraction of information on the magnetic behavior of the two different phases: the short fcc phase on the bottom of the nanowires and the predominant hcp phase. Figure 5 presents typical extrapolated FORC diagrams for the Co nanowire arrays when the external magnetic field was applied perpendicular [Fig. 5(a)] and parallel [Fig. 5(b)] to the nanowire axis. For a perpendicular applied field, only one broad

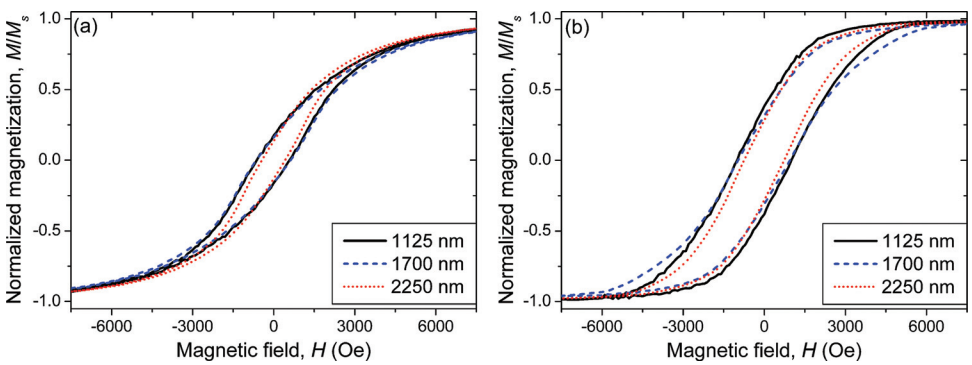

FIG. 3. (Color online) Major hysteresis curves of the Co nanowire arrays: (a) transverse (b) axial.

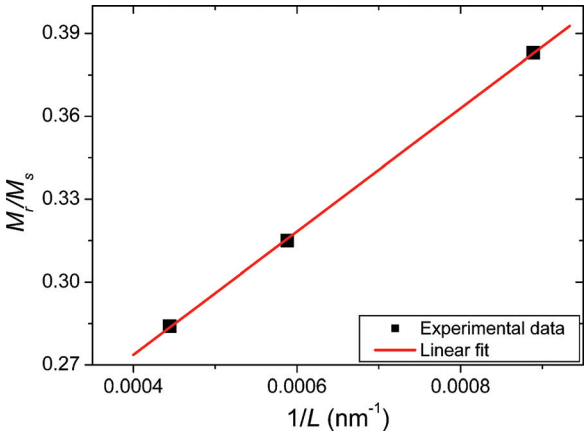

FIG. 4. (Color online) Axial normalized remanence as a function of the nanowire inverse length. The linear fit allows one to calculate the magnetic fcc phase length.

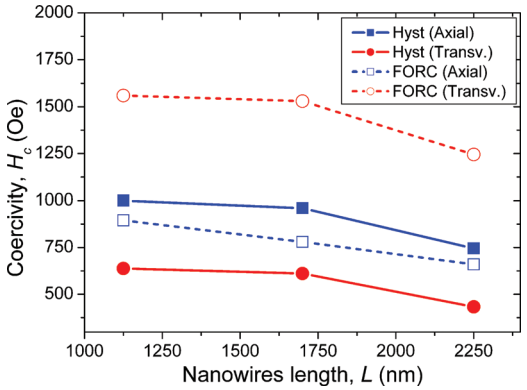

FIG. 6. (Color online) Coercivity as a function of the Co nanowire length obtained from both major hysteresis curves and FORC diagrams, for transverse and axial applied fields.

coercivity distribution, without interaction field, can be distinguished [Fig. 5(a)], which is associated with the irreversible magnetization reversal of the polycrystalline hcp phase. The magnetic easy axis of each grain (c direction) is randomly oriented in the sample plane, thus broadening the coercivity distribution. The magnetization reversal of the fcc phase appears to be completely reversible along this direction, as is expected since it corresponds to a hard axis orientation. For a parallel applied field the situation becomes more complex, and two different distributions can be clearly distinguished. The main one, elongated along the interaction field axis H_u, reflects the irreversible switching of entities submitted to an antiparallel mean interaction field, i.e., $H_{\text{int}} = kM/M_s$, where the interaction field coefficient k is negative. This feature is typical of nanowire arrays with an axial easy axis, where each nanowire reverses magnetization in a coherent way due to the dipolar interaction fields originated by the neighboring wires.[23–25] The slight counterclockwise rotation of the distribution, with regard to the parallel H_u axis, accounts for a coercivity distribution. The second feature, lying on the coercivity axis H_c, arises from a harder irreversible magnetization reversal, which may be subjected to a parallel interaction field. According to the fcc/hcp heterogeneous structure coming from the structural characterization, the FORC features can be associated with the magnetization reversal of the respective Co phase. The H_u elongated distribution can be ascribed to the predominant

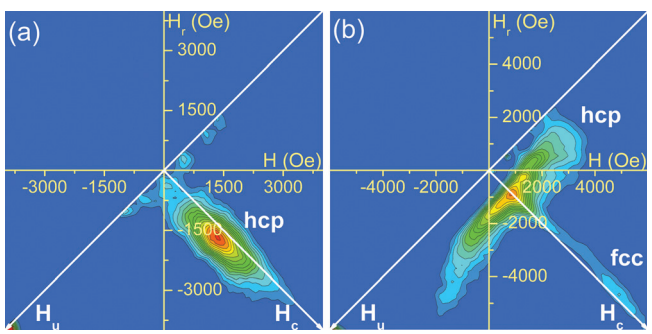

FIG. 5. (Color online) Typical extrapolated FORC diagrams ($L = 1700$ nm): (a) perpendicular (b) parallel.

hcp phase. Its anisotropy is smaller compared to the fcc one, being along the hard axis. Also, its location at the nanowire center, in height, makes it subject to the maximum dipolar interaction field. Therefore, the hcp phase will reverse its magnetization first, and it is only after this that the fcc phase can reverse, giving rise to the H_c elongated distribution. The transition from the fcc to hcp phase is probably not sharp, leading to a nanowire portion between the two phases that presents a mixture of both fcc and hcp structures. This could explain the broad coercive field distribution occurring for both phases.

In addition, the combined quantitative analysis of the hysteresis curves and the FORC diagrams reveals trends in the magnetostatic properties as a function of nanowire length. All coercivity values decrease as nanowire length increases (Fig. 6). The FORC coercivity H_c^{FORC} is defined as the position on the H_c axis of the FORC distribution maximum.[24] For a perpendicular applied field, H_c^{FORC} reflects the mean local coercivity of the hcp grains, while the hysteresis coercivity H_c^{Hyst} represents the field at which magnetization of the array vanishes. Therefore, the much higher values for H_c^{FORC} ($\sim$1500 Oe vs $\sim$600 Oe) arise from the reversible magnetization reversal of both the hcp grains and the fcc phase. For a longitudinal applied field, part of the coercivity discrepancy comes from the coercivity distribution, which rotates the FORC distribution in the presence of an antiparallel interaction field. Therefore, the exact mean hcp phase coercivity should be taken at the lower extremity of the distribution, but its numerical spreading makes this operation highly imprecise. The correlation of coercivity and nanowire length agrees with the XRD structural characterization discussed in the previous section. As nanowire length increases, hcp crystalline grain size, volume fraction, and degree of orientation of the crystalline material also increase, all of which contribute to the enhancement of the perpendicular crystalline magnetic anisotropy. For perfect perpendicular magnetic anisotropy, the longitudinal magnetization curve should present zero remanence and no hysteretic behavior. The fcc phase average coercivity is seen in the FORC diagrams and ranges from 4000 to 5000 Oe. It is not correlated to the total nanowire length, as expected, because the fcc phase length is expected to remain constant. Finally, a length-independent

interaction field of around 2300 Oe was extracted from the axial FORC diagrams.

IV. CONCLUSION

In this work, we have shown the advantages of controlling the fabrication of nanowires with two well-separated coexisting crystalline phases. Also, we have developed a characterization technique to distinguish the magnetic behavior of each contribution. Co nanowires fabricated using a single step electrodeposition technique presented a regular cylindrical shape. From the magnetic point of view, characteristics such as magnetic anisotropy strength and orientation and, consequently, other magnitudes (i. e., remanence magnetization and coercivity) can be thus tuned according to the fcc/hcp length ratio.

The Co nanowires consist of a primary fcc phase ($L_{fcc} \approx$ 260–270 nm) at the nanowire bottoms, created during the first 7 mins of electrodeposition, followed by a polycrystalline hcp phase oriented perpendicular to the nanowire axis. Moreover, the FORC method allows one to obtain specific contributions for the magnetization reversals from the fcc and hcp crystalline phases, by using simple VSM measurements. Co fcc/hcp multilayer nanowires are thus of interest for their magnetoresistance properties as well as for use in more complex spintronic devices such as spin torque oscillators.

ACKNOWLEDGMENTS

This work was supported by the Brazilian agencies FAPESP and CNpQ. M. Knobel acknowledges the Guggenheim Fellowship.

[1]D. Routkevitch, A. A. Tager, J. Haruyama, D. Almawlawi, M. Moskovits, and J. M. Xu, IEEE Trans. Electron Devices **43**, 1646 (1996).
[2]C. A. Ross, Annu. Rev. Mater. Res. **31**, 203 (2001).
[3]Z. Zhong, D. Wang, Y. Cui, M. W. Bockrath, and C. M. Lieber, Science **302**, 1377 (2003).
[4]T. Ono, H. Miyajima, K. Shigeto, K. Mibu, N. Hosoito, and T. Shinjo, Science **284**, 468 (1999).
[5]D. Atkinson, D. A. Allwood, G. Xiong, M. D. Cooke, C. C. Faulkner, and R. P. Cowburn, Nature Mater. **2**, 85 (2003).
[6]G. S. D. Beach, C. Nistor, C. Knutson, M. Tsoi, and J. Erskine, Nature Mater. **4**, 741 (2005).
[7]R. P. Cowburn and D. Petit, Nature Mater. **4**, 721 (2005).
[8]M. Hernandez-Velez, K. R. Pirota, F. Paszti, D. Navas, A. Climent, and M. Vazquez, Appl. Phys. A **80**, 1701 (2005).
[9]K. Nielsch, R. B. Wehrspohn, J. Barthel, J. Kirschner, U. Gosele, S. F. Fischer, and H. Kronmuller, Appl. Phys. Lett., **79**, 1360 (2001).
[10]K. Nielsch, R. B. Wehrspohn, J. Barthel, J. Kirschner, S. F. Fischer, H. Kronmuller, T. Schweinbock, D. Weiss, and U. Gosele, J. Magn. Magn. Mater. **249**, 234 (2002).
[11]D. J. Sellmyer, M. Zheng, and R. Skomski, J. Phys. Condens. Matter **13**, R433 (2001).
[12]R. M. Metzger, V. V. Konovalov, M. Sun, T. Xu, G. Zangari, B. Xu, M. Benakli, and W.D. Doyle, IEEE Trans. Magn. **36**, 30 (2000).
[13]R. Ferré, K. Ounadjela, J. M. George, L. Piraux, and S. Dubois, Phys. Rev. B **56** 14066 (1997).
[14]J. L. Budendorff, C. Mény, E. Beaurepaire, P. Panissod, and J. P. Bucher, Eur. Phys. J. B **17**, 635 (2000).
[15]J. Sánchez-Barriga, M. Lucas, F. Radu, E. Martin, M. Multigner, P. Marin, A. Hernando, and G. Rivero, Phys. Rev. B **80**, 184424 (2009).
[16]K. R. Pirota and M. Vazquez, Adv. Eng. Mater. **7**, 1111 (2005).
[17]I. D. Mayergoyz, J. Appl. Phys. **57**, 3804 (1985).
[18]C. R. Pike, C. A. Ross, R. T. Scalettar, and G. Zimanyi, Phys. Rev. B **71**, 134407 (2005).
[19]F. Béron, D. Menard, and Arthur Yelon, J. Appl. Phys. **103**, 07D908 (2008).
[20]D. Suess, Appl. Phys. Lett. **89**, 113105 (2006).
[21]See M. D. Vaudin, TexturePlus, http://www.ceramics.nist.gov/webbook/TexturePlus/texture.htm, 2000 for more information about this program.
[22]W. A. Dollase, J. Appl. Cryst. **19**, 267–272 (1986).
[23]F. Béron, L. Clime, M. Ciureanu, D. Ménard, R. W. Cochrane, and A. Yelon, J. Nanosci. Nanotechnol. **8**, 2944 (2008).
[24]F. Béron, L.-P. Carignan, D. Ménard, and A. Yelon, in *Electrodeposited Nanowires and Their Applications*, edited by N. Lupu (IN-TECH, Vienna, 2010).
[25]F. Béron, L. Clime, M. Ciureanu, R. W. Cochrane, D. Ménard, and A. Yelon, J. Appl. Phys. **101**, 09J107 (2007).